Estimation of reference evapotranspiration using some class-A pan evaporimeter pan coefficient estimation models in Mediterranean–Southeastern Anatolian transitional zone conditions of Turkey (#97388)

First submission

Guidance from your Editor

Please submit by **30 Mar 2024** for the benefit of the authors (and your token reward) .

Structure and Criteria
Please read the 'Structure and Criteria' page for general guidance.

Author notes
Have you read the author notes on the guidance page?

Raw data check
Review the raw data.

Image check
Check that figures and images have not been inappropriately manipulated.

If this article is published your review will be made public. You can choose whether to sign your review. If uploading a PDF please remove any identifiable information (if you want to remain anonymous).

Files
Download and review all files from the materials page.

11 Figure file(s)
5 Table file(s)
7 Raw data file(s)

For assistance email peer.review@peerj.com

Structure and Criteria

Structure your review

The review form is divided into 5 sections. Please consider these when composing your review:

1. **BASIC REPORTING**
2. **EXPERIMENTAL DESIGN**
3. **VALIDITY OF THE FINDINGS**
4. General comments
5. Confidential notes to the editor

You can also annotate this PDF and upload it as part of your review

When ready submit online.

Editorial Criteria

Use these criteria points to structure your review. The full detailed editorial criteria is on your guidance page.

BASIC REPORTING

- Clear, unambiguous, professional English language used throughout.
- Intro & background to show context. Literature well referenced & relevant.
- Structure conforms to PeerJ standards, discipline norm, or improved for clarity.
- Figures are relevant, high quality, well labelled & described.
- Raw data supplied (see PeerJ policy).

EXPERIMENTAL DESIGN

- Original primary research within Scope of the journal.
- Research question well defined, relevant & meaningful. It is stated how the research fills an identified knowledge gap.
- Rigorous investigation performed to a high technical & ethical standard.
- Methods described with sufficient detail & information to replicate.

VALIDITY OF THE FINDINGS

- Impact and novelty not assessed. *Meaningful* replication encouraged where rationale & benefit to literature is clearly stated.
- All underlying data have been provided; they are robust, statistically sound, & controlled.
- Conclusions are well stated, linked to original research question & limited to supporting results.

Standout reviewing tips

The best reviewers use these techniques

Tip	*Example*
Support criticisms with evidence from the text or from other sources	*Smith et al (J of Methodology, 2005, V3, pp 123) have shown that the analysis you use in Lines 241-250 is not the most appropriate for this situation. Please explain why you used this method.*
Give specific suggestions on how to improve the manuscript	*Your introduction needs more detail. I suggest that you improve the description at lines 57- 86 to provide more justification for your study (specifically, you should expand upon the knowledge gap being filled).*
Comment on language and grammar issues	*The English language should be improved to ensure that an international audience can clearly understand your text. Some examples where the language could be improved include lines 23, 77, 121, 128 – the current phrasing makes comprehension difficult. I suggest you have a colleague who is proficient in English and familiar with the subject matter review your manuscript, or contact a professional editing service.*
Organize by importance of the issues, and number your points	*1. Your most important issue* *2. The next most important item* *3. …* *4. The least important points*
Please provide constructive criticism, and avoid personal opinions	*I thank you for providing the raw data, however your supplemental files need more descriptive metadata identifiers to be useful to future readers. Although your results are compelling, the data analysis should be improved in the following ways: AA, BB, CC*
Comment on strengths (as well as weaknesses) of the manuscript	*I commend the authors for their extensive data set, compiled over many years of detailed fieldwork. In addition, the manuscript is clearly written in professional, unambiguous language. If there is a weakness, it is in the statistical analysis (as I have noted above) which should be improved upon before Acceptance.*

Estimation of reference evapotranspiration using some class-A pan evaporimeter pan coefficient estimation models in Mediterranean–Southeastern Anatolian transitional zone conditions of Turkey

Selçuk Usta Corresp. [1]

[1] Construction Technology/Van Vocational School, Van Yüzüncü Yıl University, Van, Turkey

Corresponding Author: Selçuk Usta
Email address: susta@yyu.edu.tr

Background. Reference evapotranspiration (ET_o), which is used as the basic data in many studies within the scope of hydrology, meteorology, irrigation and soil sciences, can be estimated by using the evaporation (E_{pan}) measured from the class-A pan evaporimeter. However, this method requires reliable pan coefficients (K_p). Many empirical models have been used to estimate these coefficients. The reliability of these models varies depending on climatic and environmental conditions. Therefore, they need to be tested in the local conditions where they will be used. This study, conducted in Kahramanmaraş, Turkey during the July–October periods of 2020 and 2021, aimed to compare Cuenca, Snyder, Wahed & Snyder, FAO-56, Modified Snyder, and Orang models and to determine their usability levels.

Methods. The K_p coefficients estimated by the models were multiplied with the daily E_{pan} values, and the daily average ET_o values were estimated on the basis of the model. Daily E_{pan} values were measured using an ultrasonic sensor sensitive to the water surface placed on the class-A pan evaporimeter. The ultrasonic sensor was managed by a Programmable Logic Controller (PLC). To enable the sensor to be managed by PLC, software was prepared using the CODESYS programming language and uploaded to the PLC. The ET_o values determined by using the FAO-56 Penman–Monteith equation were accepted as actual values. The mean absolute percentage error (MAPE) statistical approach was used to compare estimated and actual ET_o values.

Results. The nearest values to the actual ET_o values, which ranged between 2.20–8.93 mm day^{-1} in the first year and 1.77–9.60 mm day^{-1} in the second year, were estimated by the models of FAO-56 (1.91–9.15 mm day^{-1}) and Wahed & Snyder (2.07–9.89 mm day^{-1}), respectively. Using these models with the best-estimating performances, ET_o values reaching an accuracy level of 88.19% (MAPE= 11.81%) and 86.48% (MAPE= 13.52%) were obtained, respectively. The accuracy level was realised as 63.60% (MAPE= 36.40%) in the Snyder model, with the worst estimation performance. It was concluded that daily average ET_o values can be estimated with high accuracy using FAO-56 and Wahed & Snyder models in Kahramanmaraş located in the Mediterranean–Southeastern Anatolian transitional zone.

Estimation of Reference Evapotranspiration Using Some Class-A Pan Evaporimeter Pan Coefficient Estimation Models in Mediterranean–Southeastern Anatolian Transitional Zone Conditions of Turkey

Selçuk Usta[1]

[1] Construction Technology, Van Vocational School, Van Yüzüncü Yıl University, Van, Turkey

Corresponding Author:
Selçuk Usta[1]
Van Yüzüncü Yıl University Campus, Van Vocational School, Tuşba/Van, 65080, Turkey
Email address: susta@yyu.edu.tr

Abstract

Background. Reference evapotranspiration (ET_o), which is used as the basic data in many studies within the scope of hydrology, meteorology, irrigation and soil sciences, can be estimated by using the evaporation (E_{pan}) measured from the class-A pan evaporimeter. However, this method requires reliable pan coefficients (K_p). Many empirical models have been used to estimate these coefficients. The reliability of these models varies depending on climatic and environmental conditions. Therefore, they need to be tested in the local conditions where they will be used. This study, conducted in Kahramanmaraş, Turkey during the July–October periods of 2020 and 2021, aimed to compare Cuenca, Snyder, Wahed & Snyder, FAO-56, Modified Snyder, and Orang models and to determine their usability levels.

Methods. The K_p coefficients estimated by the models were multiplied with the daily E_{pan} values, and the daily average ET_o values were estimated on the basis of the model. Daily E_{pan} values were measured using an ultrasonic sensor sensitive to the water surface placed on the class-A pan evaporimeter. The ultrasonic sensor was managed by a Programmable Logic Controller (PLC). To enable the sensor to be managed by PLC, software was prepared using the CODESYS programming language and uploaded to the PLC. The ET_o values determined by using the FAO-56 Penman–Monteith equation were accepted as actual values. The mean absolute percentage error (MAPE) statistical approach was used to compare estimated and actual ET_o values.

Results. The nearest values to the actual ET_o values, which ranged between 2.20–8.93 mm day^{-1} in the first year and 1.77–9.60 mm day^{-1} in the second year, were estimated by the models of FAO-56 (1.91–9.15 mm day^{-1}) and Wahed & Snyder (2.07–9.89 mm day^{-1}), respectively. Using these models with the best-estimating performances, ET_o values reaching an accuracy level of 88.19% (MAPE= 11.81%) and 86.48% (MAPE= 13.52%) were obtained, respectively. The

accuracy level was realised as 63.60% (MAPE= 36.40%) in the Snyder model, with the worst estimation performance. It was concluded that daily average ET_o values can be estimated with high accuracy using FAO-56 and Wahed & Snyder models in Kahramanmaraş located in the Mediterranean–Southeastern Anatolian transitional zone.

Introduction

Evapotranspiration (ET) constitutes the most basic data for many studies such as determining the irrigation requirements of crops and preparing irrigation schedules, design, construction, and operation of irrigation–drainage systems, ponds, and dams, determining the amount of precipitation infiltrating into groundwater, and monitoring aridity (*Pandey et al., 2016*). ET can be most accurately measured using lysimeter systems. However, these system's installation and operational costs are high, and the measurement processes are complex and time-consuming. Therefore, the approach of estimating ET by correcting ET_o with the crop coefficient (K_c) is more preferred and widely used (*Şarlak & Bağçacı, 2020*).

Today, the most preferred method for estimating ET_o is the Penman-Monteith. This method, created in 1948, was further developed by the Food and Agriculture Organization of the United Nations (FAO) in 1998 by adapting it to the grass reference crop and making it available under the name FAO-56 modification of the Penman-Monteith (PM) equation with Irrigation and Drainage Publication No. 56 (*Allen et al., 1998*). Numerous studies have revealed that the Penman-Monteith method is capable of estimating ET_o values with high accuracy (*Lage et al., 2003*; *Jacobs et al., 2004*; *Trajković & Gocić, 2010*). As an alternative to the FAO-56 PM method, which is based on air temperature (T), relative humidity (RH), wind velocity (U_2), solar radiation (R_s), and soil heat flux (G), many empirical estimation methods based on T (*Thornthwaite, 1948*; *Blaney & Criddle, 1950*; *Hamon, 1961*), R_s (*Makkink, 1957*; *Jensen & Haise, 1963*; *Priestley & Taylor, 1972*; *Doorenbos & Pruitt, 1977*), both T and R_s (*Turc, 1961*; *Hargreaves & Samani, 1985*) have been developed. The climate data needed for both FAO-56 PM and other empirical estimation methods are measured by meteorological ground observation stations. Although these stations are not widespread enough around the world, they are mostly located in city centres. Therefore, climate data cannot be measured continuously and regularly in rural areas. This situation limits the usability of estimation methods (*El-Sebaii et al., 2009*).

Unlike the methods of lysimeter and empirical estimation, in the class-A pan evaporimeter method, the E_{pan} from the water surface is corrected by the K_p coefficient and ET_o can be estimated depending on only one parameter. Reliable K_p coefficients are needed in this method, which is widely preferred in ET_o estimation due to the low cost and simplicity of the technique used. To determine K_p coefficients, many estimation models were developed as a function of the upwind buffer zone distance (FET), U_2, and RH around the class-A pan evaporimeter (*Cuenca, 1989*; *Snyder, 1992*; *Abdel-Wahed & Snyder, 2008*; *Allen et al., 1998*; *Grismer et al., 2002*; *Orang, 1998*; *Pereira et al., 1995*; *Raghuwanshi & Wallender, 1998*). However, since these methods are compatible with the climate and environmental characteristics of the region, where they were developed, their reliability should be tested if they are used in different regions

(*Jensen et al., 1990*; *Irmak et al., 2002*). Numerous studies have been conducted in many regions with diverse climatic and environmental characteristics. In these studies, ET_o values obtained by K_p estimation models were compared with ET_o values determined using the lysimeter or empirical estimation models. *Sentelhas & Folegatti (2003)* estimated ET_o values using some K_p coefficient estimation models for a semi-arid region in Brazil and compared these values with actual ET_o values measured by a weighing lysimeter. They indicated that the Pereira and Cuenca models were the best for estimating ET_o. *Gundekar et al. (2008)*, *Kaya et al. (2012)*, and *Prandan et al. (2013)* reported that Snyder and Pereira are the models with the best and worst estimating performances, respectively, in the semi-arid conditions. *Aydın (2019)* declared that the Snyder model performed better than the Pereira model in the semi-arid Southeastern Anatolia region of Turkey. *Tya et al. (2020)* estimated the ET_o values nearest to the ET_o values obtained by the FAO-56 PM equation using the Orang model in a study conducted in semi-arid conditions of Nigeria. *Sabziparvar et al. (2010)* reported that Snyder is the model that performs best in Iran's warm-arid climate. *Irmak et al. (2002)*, *SreMaheswari & Aruna Jyothy (2017)*, *Kar et al. (2017)*, *Khobragade et al. (2019)*, and *Mahmud et al. (2020)* revealed that Snyder and Cuenca are the models with the highest estimating performance in their studies conducted in humid regions of the United States of America, India and Bangladesh, respectively. *Rodrigues et al. (2020)* developed a new model based on T, RH, R_s, and U_2 parameters in Portuguese conditions with a Mediterranean climate. They obtained determination coefficients (R^2) ranging from 0.67 to 0.74 as an expression of the statistical relationship between the ET_o values estimated with this model and the ET_o values determined using the Eddy covariance method. *Aschonitis et al. (2012)* concluded that the models with the best and worst estimating performances were Cuenca and Snyder, respectively, in their study realised in the Thessaloniki Plain of Greece, which has a semi-arid Mediterranean climate. *Koç (2022)* stated that in Adana, located in southern Turkey with a hot-summer Mediterranean climate, the models with the best and worst estimating performances were Wahed & Snyder and Snyder, respectively. Similarly, this study conducted in Kahramanmaraş with a Mediterranean climate, aimed to compare the Cuenca, Snyder, Wahed & Snyder, FAO-56, Modified Snyder, and Orang models, and to determine their usability levels in estimating daily average ET_o.

Materials & Methods

Kahramanmaraş is located between 37° 36' north latitude and 36° 55' east longitude in the Mediterranean-Southeastern Anatolian transitional zone of Turkey, and its altitude is 568 m (Fig. 1). The annual averages of the air temperature and relative humidity are 16.90 °C and 58.34%, respectively. In parts of the city with an altitude of up to 1000 meters, the Mediterranean climate is dominant, with hot and dry summers and mild and rainy winters. In parts with an altitude of more than 1000 meters, the effects of the Mediterranean mountain climate are felt, with cold and snowy winters and relatively cool summers. Kahramanmaraş, with a annual total precipitation of 721.60 mm, is located in the semi-arid climatic zone. During the May–October period, when the daily maximum air temperature varying between 26.10–36.10 °C, precipitation decreases considerably. In this period, the monthly total precipitation varying between 2.20–45.40 mm is insufficient to satisfy the crop water consumption and irrigation becomes mandatory (*Turkish State Meteorological Service, 2022*).

This study was conducted in the research field established on the Kahramanmaraş Sütçü İmam University campus, July–October periods of the 2020 and 2021. The research field is located at 37° 35' 36" north latitude and 36° 49' 20" east longitude, with an altitude of 508 m.

Firstly, the daily average ET_o values were determined by using the FAO-56 PM equation (Eq. 1). These values were accepted as actual ET_o values. The components of Eq. (1) were determined using the Irrigation and Drainage Publication No. 56 (*Allen et al., 1998*).

$$ET_o = \frac{0.408\,\Delta\,(R_n - G) + \gamma\left(\frac{900}{T + 273}\right) U_2 (e_s - e_a)}{\Delta + \gamma\,(1 + 0.34\,U_2)} \quad (1)$$

Where ET_o= reference evapotranspiration (mm day^{-1}); Δ= slope of saturation vapour pressure curve (kPa/°C^{-1}); R_n= net radiation (MJ m^{-2} day^{-1}); G= soil heat flux (MJ m^{-2} day^{-1}); γ= psychrometric constant (kPa/°C^{-1}); e_s= saturation vapour pressure (kPa); e_a= actual vapour pressure (kPa); $e_s - e_a$= vapour pressure deficit (kPa); U_2= wind velocity at 2 m above ground surface (m s^{-1}); T= daily average air temperature (°C) (*Allen et al., 1998*).

Secondly, by measuring the daily E_{pan} values from the class-A pan evaporimeter installed in the research field, the daily actual K_p coefficients were determined by Eq. (2) (*Doorenbos & Pruitt, 1977*; *Allen et al., 1998*).

$$ET_o = E_{pan} . K_p \qquad K_p = \frac{ET_o}{E_{pan}} \quad (2)$$

Where ~~K_p=~~ E_{pan}= pan evaporation (mm day^{-1}); K_p= pan coefficient.

Thirdly, the K_p coefficients were estimated using the models of Cuenca (*Cuenca, 1989*), Snyder (*Snyder, 1992*), Wahed & Snyder (*Abdel-Wahed & Snyder, 2008*), FAO-56 (*Allen et al., 1998*), Modified Snyder (*Grismer et al., 2002*) and Orang (*Orang, 1998*). These models developed as a function of the FET, U_2 and RH around the Class-A pan evaporimeter are given in Table 1. The evaporimeter used in this study was placed on dry fallow soil surrounded by green crops at an average distance of 20 m. For this reason, the FET distance was considered as 20 m.

Finally, the K_p coefficients determined using the models were multiplied by the daily E_{pan} values, and the daily ET_o values were estimated on the basis of the model. The estimated ET_o values were compared with the actual ET_o values determined by the FAO-56 PM equation. Thus, the accuracy and reliability levels of the pan coefficient estimation models have been revealed.

Daily T, RH, U_2 and R_s used as input variables in the FAO-56 PM and K_p estimation models were measured ~~with~~ the climate station given in Fig. 2. The sensors on the climate station have been managed by the PM 590 PLC.

PM 590 PLC has an SD card with 2 GB memory, 160 analog inputs, 160 analog outputs, 320 digital inputs and 240 digital outputs. It generates numerical values (NV) varying between 1–27648 for input signals varying between of 4–20 mA or 0–10 V (*ABB, 2020a*). The temperature and humidity sensors can measure with an accuracy of ±0.21 °C and ±2.50% in the ranges of 0–

50 °C and 10–90%, respectively. Similarly, solar radiation and wind velocity sensors can measure with an accuracy of 7.00 µV $Watt^{-1}$ m^{-2} and 0.10 m s^{-1} in the ranges of 0–2000 Watt m^{-2} and 0.40–30 m s^{-1}, respectively (*ONSET, 2020*; *EKO, 2020*; *NESA, 2020*). To enable the sensors to be managed by PLC, software was prepared using the CODESYS programming language and uploaded to the PLC (*ABB, 2020b*). This software measured the air temperature and relative humidity every hour on the hour, solar radiation and wind velocity every half hour during one-day periods and recorded them on the SD card on the PLC. The 24-hour period between 08:59:30 on the previous day and 08:59:30 on the next day was taken into account as a one-day period.

The temperature and humidity sensors generate output signals varying between of 4–20 mA for the values of varying between of 0–100 °C and 0–100%, respectively. These signals were firstly converted to numerical values varying between 0 to 27648 by the PLC, and then to the values of hourly temperature in °C (Eq. 3a) and hourly humidity in % (Eq. 3b) by the software. The numerical value generated by the PLC for the maximum values of temperature (100 °C) and humidity (100%) is 27648. The software determined the daily maximum and minimum values of air temperature and relative humidity by sorting the hourly temperature and humidity data, from the biggest to the smallest, at the end of the day. It calculated the arithmetic averages of these values, and determined the daily average temperature (Eq. 4a) and humidity (Eq. 4b).

$$T_h = \frac{NV.100}{27648} \quad (a) \qquad RH_h = \frac{NV.100}{27648} \quad (b) \qquad (3)$$

$$T = \frac{T_{max} + T_{min}}{2} \quad (a) \qquad RH = \frac{RH_{max} + RH_{min}}{2} \quad (b) \qquad (4)$$

Where T_h= hourly air temperature (°C); NV= numerical value generated by PLC (0-27648); RH_h= hourly relative humidity (%); T_{max}= daily maximum air temperature (°C); T_{min}= daily minimum air temperature (°C); RH_{max}= daily maximum relative humidity (%); RH_{min}= daily minimum relative humidity (%); T= daily average air temperature (°C); RH= daily average relative humidity (%).

The solar radiation and wind velocity sensors generate output signals varying between of 0–10 V for the values of varying between of 0–2000 Watt m^{-2} and 0.28–50 m s^{-1}, respectively. The signals generates by the radiation sensor were firstly converted to numerical values varying between 0 to 27648 by the PLC, and then to the half-hourly solar radiation values by the software (Eq. 5a). Similarly, the signals generates by the wind velocity sensor were firstly converted to numerical values varying between 0 to 5530 by the PLC, and then to the half-hourly wind velocity values by the software (Eq. 5b). The numerical values generated by the PLC for the maximum values of the solar radiation (2000 Watt m^{-2}) and wind velocity (50 m s^{-1}) are 27648 and 5530, respectively.

$$RS_{h/2} = \frac{NV.2000}{27648} \quad (a) \qquad U_{h/2} = \frac{NV.50}{5530} \quad (b) \qquad (5)$$

Where $RS_{h/2}$= half-hourly solar radiation (Watt m^{-2}); $U_{h/2}$= half-hourly wind velocity (m s^{-1}).

The software summed the half-hourly solar radiation and wind velocity data at the end of the day, and obtained the daily total values of the solar radiation and wind velocity. It divided the total values by the number of measurements (48), and determined the daily average solar radiation (Eq. 6a) and wind velocity (Eq. 6b). The solar radiation sensor measures in Watt m^{-2} unit. However, solar radiation is used in unit of MJ m^{-2} day^{-1} in the FAO-56 PM equation. For this reason, the values measured in Watt m^{-2} unit were multiplied by the coefficient of 0.0864 and converted to MJ m^{-2} day^{-1} unit.

$$R_s = \left(\frac{\Sigma RS_{h/2}}{48}\right)0.0864 \quad (a) \qquad U_2 = \frac{\Sigma U_{h/2}}{48} \quad (b) \qquad (6)$$

Where $\Sigma RS_{h/2}$= daily total solar radiation (MJ m^{-2} day^{-1}); $\Sigma U_{h/2}$= daily total wind velocity (m s^{-1}); R_s= daily average solar radiation (MJ m^{-2} day^{-1}); U_2= daily average wind velocity (m s^{-1}).

Daily E_{pan} values were measured using an ultrasonic sensor sensitive to the water surface placed on the class-A pan evaporimeter given in Fig. 3.

To enable the ultrasonic and pressure sensors and solenoid valve to be managed by PLC, software was prepared using the CODESYS programming language and uploaded to the PLC (*ABB, 2020b*). This software performed the measurements for one-day periods. The 24-hour period between 08:59:30 on the previous day and 08:59:30 on the next day was considered as a one-day period. The ultrasonic sensor generates output signals varying between 4–20 mA for distances varying between 0–500 mm (*PEPPERLY, 2020*). These signals generated by the sensor for the height (0–500 mm) between itself and the water surface were firstly converted to numerical values varying between 0 to 27648 by the PLC, and then to the actual height distance values in mm by the software (Eq. 7). The numerical value generated by the PLC for the maximum height (H= 500 mm) is 27648. Finally, the software determined the water level in the Class-A pan evaporimeter by using Eq. (8) and recorded it on the SD card. Daily E_{pan} was determined by subtracting the water levels measured at the beginning and end of a one-day period (Eq. 9). Measuring the water level in the evaporimeter was started when the water level was 200 mm. When the water level falls below 150 mm, the PLC opens the solenoid valve, allowing water to be supplied to the evaporimeter until the water level reaches 200 mm. The valve is automatically closed by the PLC, when the water level reaches 200 mm.

$$d = \frac{NV.500}{27648} \qquad (7)$$

$$D = 500 - d \qquad (8)$$

$$E_{pan} = D_{beg.} - D_{end} \qquad (9)$$

Where d= the height distance between the ultrasonic sensor and the water surface (mm); D= the water level in the pan evaporimeter (mm); $D_{beg.}$= the water level measured at the beginning of a one-day period (mm); D_{end} = the water level measured at the end of a one-day period (mm);

The daily average actual and estimated ET_o values were compared using the statistical approaches of the mean absolute error, mean absolute percentage error, and root mean square error. These errors were determined using Eq. (10-12), respectively. Mean absolute percentage error was taken into account in revealing the accuracy levels of the ET_o values estimated using the daily average K_p coefficients determined by the models. The accuracy of the estimated ET_o values; mean absolute percentage error was evaluated as "excellent" if it was less than 10%, "good" if it was between 10–20%, "reasonable" if it was between 20–50%, and "inaccurate" if it was more than 50% (*Lewis, 1982*). To reveal the level of statistical relationship between ET_o values of the actual and estimated, regression analyses were performed using the Microsoft Excel program, and the results were discussed (Eq. 13).

$$MAE = \frac{1}{n}\Sigma_{i:1}^{n}\left(\left|X_i - Y_i\right|\right) \quad (10)$$

$$MAPE = \frac{1}{n}\Sigma_{i:1}^{n}\left(\frac{\left|X_i - Y_i\right|}{X_i}100\right) \quad (11)$$

$$RMSE = \sqrt{\frac{1}{n}\Sigma_{i:1}^{n}\left(X_i - Y_i\right)^2} \quad (12)$$

$$R^2 = \frac{\left[\Sigma_{i:1}^{n}\left(X_i - \hat{X}\right)\left(Y_i - \hat{Y}\right)\right]^2}{\Sigma_{i=1}^{n}\left(X_i - \hat{X}\right)^2 \Sigma_{i=1}^{n}\left(Y_i - \hat{Y}\right)^2} \quad (13)$$

Where MAE= mean absolute error (mm day^{-1}); MAPE= mean absolute percentage error (%); RMSE= root mean square error (mm day^{-1}); X_i and Y_i = actual and estimated ET_o values (mm day^{-1}); $\hat{X}$ and $\hat{Y}$ = averages of the actual and estimated ET_o values (mm day^{-1}); R^2= determination coefficient; n= number of observations (123 days).

Results and Discussion

The daily average air temperature and relative humidity values were given in Fig. 4. The daily average air temperature varied between 17.66–30.10 °C and 15.47–33.90 °C in 2020 and 2021, respectively. Relative humidity tended to decrease in the July–August period, when the temperature showed an increasing trend, and to increase in the September–October period, when the temperature showed a decreasing trend. The daily average relative humidity ranged between 24.50–61.30% and 30.20–67.80% in 2020 and 2021, respectively.

The daily average wind velocity values ranged between 0.40–4.23 m s^{-1} and 0.43–4.65 m s^{-1} in 2020 and 2021, respectively. Solar radiation, which showed a decreasing trend during the July–October period similarly wind velocity, ranged between 10.51–30.23 MJ m^{-2} day^{-1} and 10.40–29.23 MJ m^{-2} day^{-1}, respectively (Fig. 5).

The daily average actual ET_o and daily total E_{pan} values were given in Fig. 6. The ET_o values varied between 2.20–8.93 mm day^{-1} and 1.77–9.60 mm day^{-1} in the July–October periods of 2020 and 2021, respectively. The E_{pan} values varied between 3.00–16.00^{-1} mm day^{-1} and 3.00–15.00 mm day^{-1}, respectively. It has been observed that the amounts of ET_o and E_{pan} realised on the days when the air temperature, wind velocity, and solar radiation were at high levels and the relative humidity was at low levels, were higher than the other days. As can be seen in the graphs in Fig. 6, both ET_o and E_{pan} values showed a decreasing trend during the July–October period. The daily ET_o and E_{pan} were increased to maximum levels in the last period of July and the first and second periods of August. They were decreased to minimum levels in the last period of October. The rate of explaining the change in daily average ET_o values with daily total E_{pan} values was determined as 83% (R^2= 0.83) and 78% (R^2= 0.78) for the July–October periods of 2020 and 2021, respectively.

The daily average actual and estimated K_p coefficients were given in Fig. 7. Actual coefficients ranged between 0.38–0.88 in the first year and 0.35–1.08 in the second year. Seasonal average coefficients were determined as 0.60 and 0.65, respectively. Similarly, the daily coefficients estimated using the Cuenca, FAO-56, Modified Snyder, Orang, Snyder and Wahed & Snyder models for both years varied between 0.61–0.77, 0.52–0.71, 0.67–0.78, 0.67–0.78, 0.72–0.91, and 0.60–0.70, respectively. Seasonal coefficients were determined as 0.70, 0.60, 0.62, 0.72, 0.81 and 0.65 respectively. It has been observed that the K_p coefficients estimated using the models of Modified Snyder and Orang were very similar to each other.

The monthly average K_p coefficients for the July–October periods of 2020 and 2021 were given in Table 2. The actual coefficients were determined as 0.62 for July, 0.60 for August, 0.61 for September and 0.58 for October in the first year. The same coefficients were obtained for the second year as 0.67, 0.65, 0.67 and 0.61, respectively. The nearest values to the actual coefficients were estimated by the FAO-56 (0.57–0.63) in the first year and by the Wahed & Snyder (0.64–0.65) in the second year. The furthest values were estimated by the Snyder (0.80–0.82) in both years. Generally, it has been observed that the K_p coefficient changes directly proportional to the humidity, which tends to increase during the July–October period, and inversely proportional to the wind speed, which tends to decrease in the same period.

The daily average actual ET_o values calculated using the FAO-56 PM equation and the daily average ET_o values estimated using the K_p coefficients determined by the models of Cuenca, FAO-56, Modified Snyder, Orang, Snyder and Wahed & Snyder were given in Fig. 8. Using these models, daily ET_o values ranging from 2.09–10.97 mm day^{-1}, 1.91–9.15 mm day^{-1}, 2.15–11.34 mm day^{-1}, 2.16–11.40 mm day^{-1}, 2.43–12.82 mm day^{-1} and 1.93–10.18 mm day^{-1} were estimated, respectively, in the first year. The seasonal average values were determined as 6.83 mm day^{-1}, 5.83 mm day^{-1}, 7.07 mm day^{-1}, 7.10 mm day^{-1}, 7.96 mm day^{-1} and 6.35 mm day^{-1}, respectively. In the same year, the daily actual ET_o values varied between 2.20–8.93 mm day^{-1}. The actual seasonal average ET_o was determined as 5.91 mm day^{-1}. The nearest values to the actual ET_o values were estimated by the FAO-56, and the furthest values were estimated with the Snyder in the first year. Except for the FAO-56, the nearest values to the actual ET_o values were obtained by using the models of Wahed & Snyder, Cuenca, Modified Snyder, Orang and Snyder, respectively.

In the second year, using the models of Cuenca, FAO-56, Modified Snyder, Orang, Snyder and Wahed & Snyder daily average ET_o values ranging from 2.30–10.80 mm day^{-1}, 2.08–8.70 mm day^{-1}, 2.31–11.01 mm day^{-1}, 2.32–11.07 mm day^{-1}, 2.71–12.57 mm day^{-1} and 2.07–9.89 mm day^{-1} were estimated, respectively. The seasonal average values were determined as 6.56 mm day^{-1}, 5.57 mm day^{-1}, 6.77 mm day^{-1}, 6.80 mm day^{-1}, 7.63 mm day^{-1} and 6.08 mm day^{-1}, respectively. In the same year, the daily average actual ET_o values ranged between 1.77–9.60 mm day^{-1}. The seasonal average actual ET_o was determined as 6.03 mm day^{-1}. Unlike the first year, the nearest values to the actual ET_o values were estimated by Wahed & Snyder in the second year. The furthest values were estimated with the Snyder as in the first year. Except for the Wahed & Snyder in the second year, the nearest values to the actual ET_o values were estimated by using the models of FAO-56, Cuenca, Modified Snyder, Orang, and Snyder, respectively, as in the first year. Considering the results obtained for both years, it has been seen that the nearest values to the actual ET_o values can be estimated in Kahramanmaraş conditions using the models of Wahed & Snyder and FAO-56, which have similar performances. The values estimated with the models of Modified Snyder and Orang showed a very high level of similarity, for both years. As an indicator of the statistical relationship between actual and estimated daily ET_o values, R^2 coefficients ranged between 0.83–0.87 in the first year (Fig. 9) and 0.72–0.77 in the second year (Fig. 10) were obtained.

The monthly averages of the actual and estimated daily ET_o values and the MAE, MAPE, and RMSE errors calculated as an expression of the deviation between these values were given in Tables 3 and 4, respectively. The daily average ET_o values with the lowest errors in the first year were estimated using the FAO-56 model. The monthly average MAE, MAPE, and RMSE errors determined for this model, which has the best-estimating performance, varied between 0.56–0.68 mm day^{-1}, 8.79–18.78% and 0.66–0.93 mm day^{-1}, respectively. Seasonal average errors for the July–October period were realised as 0.62 mm day^{-1}, 11.81% and 0.79 mm/day, respectively. The daily ET_o values with the highest errors were estimated using the Snyder model. The MAE, MAPE and RMSE errors obtained for this model, which has the worst estimation performance, varied between 1.35–2.55 mm day^{-1}, 33.58–42.95% and 1.53–2.79 mm day^{-1}, respectively. Seasonal average errors were realised as 2.05 mm day^{-1}, 36.40% and 2.28 mm day^{-1}, respectively. The model that showed the nearest performance to FAO-56 was Wahed & Snyder. The MAE, MAPE and RMSE errors calculated for this model, ranged between 0.62–0.90 mm day^{-1}, 9.82–20.52% and 0.72–1.05 mm day^{-1}, respectively. Seasonal average errors were determined as 0.71 mm day^{-1}, 13.52% and 0.87 mm day^{-1}, respectively. Using the FAO-56 and Wahed & Snyder, daily average ET_o values were estimated with accuracy rates of 88.19% (MAPE= 11.81%) and 86.48% (MAPE= 13.52%), respectively, in the first year. The accuracy rate was obtained as 81.13% (MAPE= 18.87%), 77.82% (MAPE= 22.18%), 77.28% (MAPE= 22.72%) and 63.60% (MAPE= 36.40%) for the Cuenca, Modified Snyder, Orang, and Snyder, respectively. The accuracy of the estimated ET_o values was determined as "good" (MAPE= 10–20%) for FAO-56, Wahed & Snyder, Cuenca, and "reasonable" (MAPE= 20–50%) for other models.

The daily average ET_o values with the lowest and highest errors in the second year were estimated using the models of Wahed & Snyder and Snyder, respectively. The monthly average MAE, MAPE and RMSE errors determined for the Wahed & Snyder, which has the best-estimating performance, varied between 0.56–1.03 mm day^{-1}, 10.11–19.14% and 0.75–1.22 mm day^{-1}, respectively. The same errors varied between 1.17–1.96 mm day^{-1}, 22.91–41.82% and 1.39–2.34 mm day^{-1}, respectively, for the Snyder, which has the worst estimation performance. Seasonal average errors were obtained as 0.84 mm day^{-1}, 15.28%, 1.06 mm day^{-1} for Wahed & Snyder and as 1.71 mm day^{-1}, 31.41%, 2.08 mm day^{-1}for Snyder. The FAO-56 model, which had the best estimating performance in the first year, was the model nearest in performance to Wahed & Snyder in the second year. Seasonal average MAE, MAPE and RMSE were calculated for this model as 0.93 mm day^{-1}, 16.28% and 1.20 mm day^{-1}, respectively. In the second year, the accuracy rates of the ET_o values estimated using the Wahed & Snyder, FAO-56, Cuenca, Modified Snyder, Orang and Snyder were obtained as 84.72% (MAPE= 15.28%), 83.72% (MAPE= 16.28%), 81.54% (MAPE= 18.46%), 79.93 % (MAPE= 20.07%), 79.55% (MAPE= 20.45%), and 68.59% (MAPE= 31.41%), respectively. The accuracy of the estimated ET_o values was determined as "good" (MAPE= 10–20%) for Wahed & Snyder, FAO-56, Cuenca, and "reasonable" (MAPE= 20–50%) for other models.

The monthly total values of the daily average ET_o values estimated using the models were given in Fig. 11. The monthly total ET_o, which showed a decreasing trend during the July–October period, reached its maximum level in July and decreased to its minimum level in October. The monthly total actual ET_o values ranged between 101.22–236.26 mm and 99.13–256.43 mm, respectively, during the July–October periods of 2020 and 2021. Seasonal total actual ET_o values were realised as 727.38 mm, and 741.48 mm, respectively. The nearest values to the actual total values were obtained with the FAO-56 (716.80 mm) in the first year and Wahed & Snyder (747.64 mm) in the second year. MAPE was determined as 1.45% for FAO-56 in the first year and 0.83% for Wahed & Snyder in the second year. The furthest values to the actual seasonal total ET_o values were obtained with the Snyder in both years. The seasonal total ET_o values determined using this model were obtained as 979.03 mm in the first year and 938.75 mm in the second year. For this model, which has the worst estimation performance, MAPE was realised as 34.60% in the first year and 26.61% in the second year (Table 5).

Gundekar et al. (2008), *Sabziparvar et al. (2010)*, *Prandan et al. (2013)*, *Kaya et al. (2012)*, *Aydın (2019)* and *Tya et al. (2020)* reported that Snyder is the model with the best-estimating performance in semi-arid climate conditions. Similarly *Irmak et al. (2002)*, *SreMaheswari & Aruna Jyothy (2017)*, *Tabari el al. (2013)*, *Kar et al. (2017)*, *Khobragade et al. (2019)* and *Mahmud et al. (2020)* stated that Snyder and Cuenca are the models with the best-estimating performance in humid climatic conditions. The Snyder model, which generally has the best-estimating performance in semi-arid and humid climatic conditions, showed the worst performance (MAE= 2.05 mm day^{-1}, MAPE= 36.40%, RMSE= 2.28 mm day^{-1}) in this study conducted in Kahramanmaraş which has a semi-arid Mediterranean climate. The accuracy ranking of the six pan coefficient estimation models considered in this study, where FAO-56 (MAE= 0.62 mm day^{-1}, MAPE= 11.81%, RMSE= 0.79 mm day^{-1}) and Wahed & Snyder (MAE= 0.71 mm day^{-1}, MAPE= 13.52%, RMSE= 0.87 mm day^{-1}) models have the best-estimating performance, was as follows. FAO-56> Wahed & Snyder> Cuenca> Modified Snyder> Orang> Snyder. Similarly *Aschonitis et al. (2012)* declared that the models with the best and worst estimating performances were Cuenca (MAE= 0.14 mm day^{-1}, RMSE= 0.61 mm day^{-1}) and Snyder (MAE= 2.53 mm day^{-1}, RMSE= 2.73 mm day^{-1}), respectively, in their study conducted in the Thessaloniki plain of Greece, where has a semi-arid Mediterranean climate. The accuracy ranking of the seven models discussed in this study, in which Wahed & Snyder and FAO-56 models were not evaluated, was as follows. Cuenca > Raghuwanshi & Wallender> Allen & Pruitt> Pereira> Orang > Snyder. In another study conducted in Mediterranean climate conditions, *Koç (2022)* reported that Wahed & Snyder was the best performing model (MAE= 0.43 mm day^{-1}, RMSE= 0.55 mm day^{-1}) and Orang was the worst performing model (MAE= 1.81 mm day^{-1}, RMSE= 1.87 mm day^{-1}) in Adana, 195 km from Kahramanmaraş. The accuracy ranking of the eight models discussed in this study, was as follows. Wahed & Snyder> Modified Snyder> Cuenca> Raghuwanshi & Wallender> Pereira> Allen & Pruitt> Snyder> Orang. Using the Wahed & Snyder model in Adana conditions, monthly average K_p coefficients were estimated as 0.65, 0.65, 0.64 and 0.63 for the months of July, August, September and October, respectively. Similarly, using the same model, the K_p coefficients of 0.65, 0.64, 0.64 and 0.65 were obtained for the same months in Kahramanmaraş conditions.

Conclusions

This study evaluated six pan coefficient estimation models, Cuenca, Snyder, Wahed & Snyder, FAO-56, Modified Snyder, and Orang in Kahramanmaraş, Turkey conditions. During the July–October periods of 2020 and 2021, the K_p coefficients estimated using these models were multiplied by the daily E_{pan} values and the daily average ET_o values were estimated on the basis of the model. Daily E_{pan} values were measured using an ultrasonic sensor sensitive to water level. The ET_o values determined using the FAO-56 PM equation were accepted as actual values. The daily average ET_o values estimated by the models were compared with the actual ET_o values, and their usability levels were revealed. The models of FAO-56 and Wahed & Snyder estimated the nearest ET_o values to the actual ET_o values. Using these models with the best-estimating performances, ET_o values reaching an accuracy level of 88.19% (MAPE= 11.81%) and 86.48% (MAPE= 13.52%) were obtained, respectively. The differences between the ET_o values estimated by these models and the actual ET_o values were not statistically significant (P> 0.05, n=123). The Snyder model estimated the furthest ET_o values to the actual ET_o values. The accuracy level was realised as 63.60% (MAPE= 36.40%) in this model with the worst estimation performance. The models of Cuenca, Modified Snyder and Orang showed similar performances. It was concluded that daily average ET_o values with high accuracy can be estimated by using FAO-56 and Wahed & Snyder models in Kahramanmaraş which has a semi-arid Mediterranean climate.

References

ABB. 2020a. Detailed information for: PM590 ETH. *Available at https://new.abb.com/products/tr/1SAP150000R0271/pm590-eth* (accessed 22 March 2020).

ABB. 2020b. Automation Builder V1.2.2 basic software installation. *Available at https://new.abb. com/plc/automationbuilder/platform/software* (accessed 14 April 2020).

Abdel-Wahed MH, Snyder RL. 2008. Simple equation to estimate reference evapotranspiration from evaporation pans surrounded by fallow soil. *Journal of Irrigation and Drainage Engineering* **134(4):**425–429 DOI 10.1061/(ASCE)0733-9437(2008)134:4(425).

Allen RG, Pereire LS, Raes D, Smith M. 1998. Crop evapotranspiration guidelines for computing crop water requirements. FAO Irrigation and Drainage. Paper (56). FAO, Rome.

Aschonitis VG, Antonopoulos VZ, Papamichail DM. 2012. Evaluation of pan coefficient equations in a semi-arid Mediterranean environment using the ASCE Standardized Penman-Monteith method. *Journal of Agricultural Sciences* **3(1):**58–65 DOI 10.4236/as.2012.31008.

Aydın Y. 2019. Determination of reference ET_o by using different K_p equations based on class A pan evaporation in Southeastern Anatolia Project (GAP) region. *Applied Ecology and Environmental Research* **17(6):**15117–15129 DOI 10.15666/aeer/1706_1511715129.

Blaney HF, Criddle WD. 1950. Determining water requirements in irrigated areas from climatological irrigation data. United States Soil Conservation Service. Technical Paper (96). Washington, DC.

Cuenca RH. 1989. *Irrigation system design: an engineering approach*. Prentice Hall, Englewood Cliffs. 552. Evapotranspiration. Water Resources Bulletin 10(3):486–498.

Doorenbos J, Pruitt WO. 1977. Guidelines for predicting crop water requirements. FAO Irrigation and Drainage. Paper (24). FAO, Rome.

EKO. 2020. Pyranometers. *Available at https://www.ekoinstruments.com/eu/categories/products /pyranometers* (accessed 25 March 2020).

El-Sebaii AA, Al-Hazmi FS, Al-Ghamdi AA, Yaghmour SJ. 2010. Global, direct and diffuse solar radiation on horizontal and tilted surfaces in Jeddah, Saudi Arabia. *Applied Energy* **87(2):**568–576 DOI 10.1016/j.apenergy.2009.06.032.

Grismer ME, Orang M, Snyder R, Matyac R. 2002. Pan evaporation to reference evapotranspiration conversion methods. *Journal of Irrigation and Drainage Engineering* **128(3):**180–184 DOI 10.1061/(ASCE)0733-9437(2002)128:3(180).

Gundekar HG, Khodke UM, Sarkar S, Rai RK. 2008. Evaluation of pan coefficient for reference crop evapotranspiration for semi-arid region. *Irrigation Science* **26(2):**169–175 DOI 10.1007/s00271-007-0083-y.

Hamon WR. 1961. Estimating potential evapotranspiration. *Journal of the Hydraulics Division, Proceedings of the American Society of Civil Engineers* **87:**107–120.

Hargreaves GL, Samani ZA. 1985. Reference crop evapotranspiration from temperature. *Applied Engineering in Agriculture* **1(2):** 96–99 DOI: 10.13031/2013.26773.

Irmak S, Haman DZ, Jones JW. 2002. Evaluation of Class A Pan coefficients for estimating reference evapotranspiration in humid location. *Journal of Irrigation and Drainage Engineering* **128(3):**153–159 DOI 10.1061/(ASCE)0733-9437(2002)128:3(153).

Jacobs JM, Anderson MC, Friess LC, Diak GR. 2004. Solar radiation long wave radiation and emergent wetland evapotranspiration estimates from satellite data in Florida, USA. *Hydrological Sciences–Journal–des Sciences Hydrologiques* **49(3):**461–476 DOI 10.1623/hysj.49.3.461.54352.

Jensen ME, Haise HR. 1963. Estimating evapotranspiration from solar radiation. *Journal of Irrigation and Drainage Division* **89:**15–41.

Jensen ME, Burman RD, Allen RG. 1990. Evapotranspiration and irrigation water requirements. American Society of Civil Engineers (ASCE). Technical Report (70). New York.

Kar SK, Nema AK, Mishra CD, Sinha BL. 2017. Evaluation of class-a pan coefficient models for estimation of reference crop evapotranspiration for dry sub-humid climates. *Journal of Agricultural Engineering* **57(3):**67–74.

Kaya S, Evren S, Daşcı E, Bakır H, Adıgüzel MC. 2012. Estimation of reference evapotranspiration using pan evaporation under the Iğdır Plain conditions. *Turkish Journal of Nature and Science* **1(1):**7–14.

Khobragade SD, Semwal P, Kumar ARS, Nainwal HC. 2019. Pan coefficients for estimating open-water surface evaporation for a humid tropical monsoon climate region in India. *Journal of Earth System Science* **128:**175 DOI 10.1007/s12040-019-1198-2.

Koç DL. 2022. Assessment of pan coefficient models for the estimation of the reference evapotranspiration in a Mediterranean environment in Turkey. *PeerJ* 10:e13554 DOI 10.7717/peerj.13554.

Lage M, Bamouh A, Karrou M, El Mourid M. 2003. Estimation of rice evapotranspiration using a microlysimeter technique and comparison with FAO Penman-Monteith and Pan evaporation methods under Moroccan conditions. *Agronomie* **23(7):**625–631 DOI 10.1051/agro:2003040.

Lewis CD. 1982. *Industrial and business forecasting methods: a practical guide to exponential smoothing and curve fitting*. London: Butterworths Scientific.

Mahmud K, Siddik S, Khatun K, Islam T. 2020. Performance evaluation of Class A Pan coefficient models to estimate reference evapotranspiration in Mymensingh region of Bangladesh. *Journal of Bangladesh Agricultural University* **18(3):**742–750 DOI 10.5455/JBAU.101511.

Makkink GF. 1957. Testing the Penman formula by means of lysimeters. *Journal of the Institution of Water Engineers* **11:**277–288.

NESA. 2020. Wind speed sensor. *Available at https://www.nesasrl.eu/wpcontent/uploads/2022/12/3.VV1VV1R_EN.pdf* (accessed 23 March 2020).

ONSET. 2020. Temperature/RH smart sensor. *Available at https://www.onsetcomp.com/files/manual_pdfs/previous/11427-N%20MAN-STHB.pdf* (accessed 27 March 2020).

Orang M. 1998. Potential accuracy of the popular non-linear regression equations for estimating pan coefficient values in the original and FAO-24 tables. Unpublished California Department of Water Resources Report. Sacramento, USA.

Pandey PK, Dabral PP, Pandey V. 2016. Evaluation of reference evapotranspiration methods for the northeastern region of India. *International Soil and Water Conservation Research* **4(1):**52–63 DOI 10.1016/j.iswcr.2016.02.003.

PEPPERLY. 2020. Ultrasonic sensor. *Available at https://files.pepperlfuchs.com/webcat/navi/productInfo/pds/133053_eng.pdf?v=20230527160942* (accessed 10 April 2020).

Pereira AR, Nova NA, Pereira AS, Barbieri V. 1995. A model for the Class A Pan coefficient. *Agricultural and Forest Meteorology* **76(2):**75–82 DOI 10.1016/0168-1923(94)02224-8.

Pradhan S, Sehgal VK, Das DK, Bandyopadhyay KK, Singh R. 2013. Evaluation of pan coefficient methods for estimating FAO-56 reference crop evapotranspiration in a semi-arid environment. *Journal of Agrometeorology* **15(1):**90–93.

Priestley CHB, Taylor RJ. 1972. On the assessment of surface heat flux and evaporation using large scale parameters. *Monthly Weather Review* **100:**81–92.

Raghuwanshi NS, Wallender WW. 1998. Converting from pan evaporation to evapotranspiration. *Journal of Irrigation and Drainage Engineering* **124(5):**275–277 DOI 10.1061/(ASCE)0733-9437(1998)124:5(275).

Rana G, Katerji N. 2000. Measurement and estimation of actual evapotranspiration in the field under Mediterranean climate: a review. *European Journal of Agronomy* **13:**125–153 DOI 10.1016/S1161-0301(00)00070-8.

Rodrigues CM, Moreira M, Guimarães RC, Potes M. 2020. Reservoir evaporation in a Mediterranean climate: comparing direct methods in Alqueva Reservoir, Portugal. *Hydrology and Earth System Sciences* **24:**5973–5984 DOI 10.5194/hess-24-5973-2020.

Sabziparvar AA, Tabari H, Aeini A, Ghafouri M. 2010. Evaluation of class A pan coefficient models for estimation of reference crop evapotranspiration in cold semi-arid and warm arid climates. *Water Resources Management* **24(5):**909–920 DOI 10.1007/s11269-009-9478-2.

Sentelhas PC, Folegatti MV. 2003. Class A pan coefficients (K_p) to estimate daily reference evapotranspiration (ET_o). *Revista Brasileira de Engenharia Agricola e Ambiental* **7(1):**111–115 DOI 10.1590/S1415-43662003000100018.

Snyder RL. 1992. Equation for evaporation pan to evapotranspiration conversions. *Journal of Irrigation and Drainage Engineering* **118(6):**977–980 DOI 10.1061/(ASCE)0733-9437(1992)118:6(977).

SreeMaheswari CH, Jyothy SA. 2017. Evaluation of class A pan coefficient models for estimation of reference evapotranspiration using Penman-Monteith method. *International Journal of Science Technology & Engineering* **3(1):**90–94.

Şarlak N, Bağçacı SÇ. 2020. The assesment of empirical potential evapotranspiration methods: A case study of Konya Closed Basin. *Turkish Journal of Civil Engineering* **31(1):**9755–9772 DOI 10.18400/TEKDERG.408019.

Tabari H, Grismer ME, Trajkovic S. 2013. Comparative analysis of 31 reference evapotranspiration methods under humid conditions. *Irrigation Science* **31:**107–117 DOI 10.1007/s00271-011-0295-z.

Thornthwaite CW. 1948. An approach toward a rational classification of climate. *Geographical Review* **38:**55–94 DOI 10.2307/210739.

Trajković S, Gocić M. 2010. Comparison of some empirical equations for estimating daily reference evapotranspiration. *Facta Universitatis – Series Architecture and Civil Engineering* **8(2):**163–168 DOI 10.2298/FUACE1002163T.
Turc L. 1961. Water requirements assessment of irrigation, potential evapotranspiration: Simplified and updated climatic formula. *Annuaire Agronomie* **12:**13–49.
Turkish State Meteorological Service. 2022. Kahramanmaraş province climate data. General directorate of state meteorology data center, Ankara.
Tya TSK, Sunday C, Vanke I. 2020. Evaluation of class A pan coefficient models for estimation of crop reference evapotranspiration for Geriyo Irrıgation Scheme, Yola, Nigeria. *FUW Trends in Science & Technology Journal* **5(3):**871–875.

Figure 1

Geographical location of Kahramanmaraş in Turkey map

(Map credit: https://s.milimaj.com/others/image/harita/kahramanmaras-ili-haritasi.png).

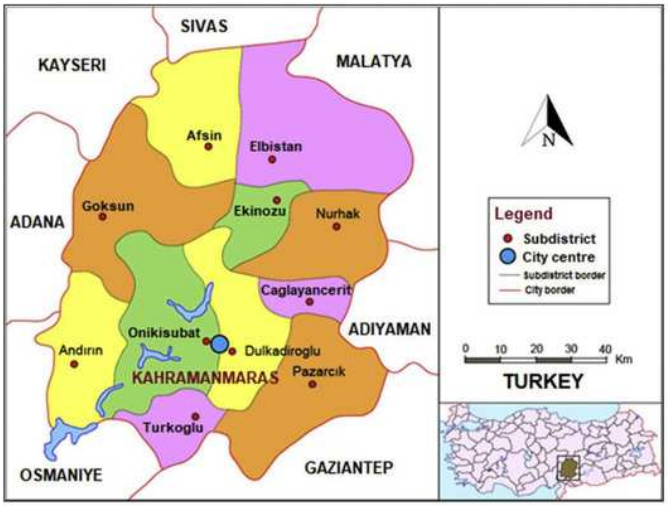

Figure 1 Geographical location of Kahramanmaraş in Turkey map (Map credit: https://s.milimaj.com/others/image/harita/kahramanmaras-ili-haritasi.png).

Figure 2

PLC controlled climate station.

This station consists of sensors wind velocity (1), solar radiation (2), air temperature–relative humidity (3), wind direction (4) and precipitation (5). These sensors were mounted on a platform (6) made of steel pipe profile.

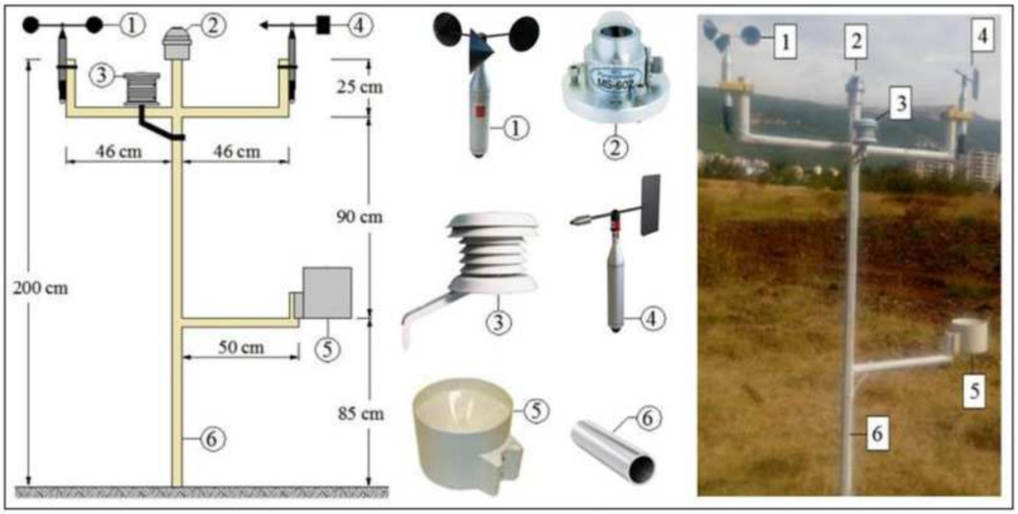

Figure 2 PLC controlled climate station. This station consists of sensors wind velocity (1), solar radiation (2), air temperature–relative humidity (3), wind direction (4) and precipitation (5). These sensors were mounted on a platform (6) made of steel pipe profile.

Figure 3

PLC controlled class-A pan evaporimeter.

This evaporimeter (2) was sited on a 10 cm high wooden frame (1) placed on dry fallow soil surrounded by green crops. The pipes of the water inlet (3) and discharge (4) were placed on the bottom of the evaporimeter. Both of these pipes have a diameter of ½''. A solenoid valve was connected to the water inlet pipe. The E_{pan} values can be measured separately by using a pressure sensor (5) placed on the discharge pipe or an ultrasonic sensor (8) sensitive to the water surface. The E_{pan} values measured by the ultrasonic sensor were used in this study. This sensor was placed at a height of 500 mm, coinciding with the centre of the evaporimeter, by means of a strut (7) with a height adjustment screw (6) on it.

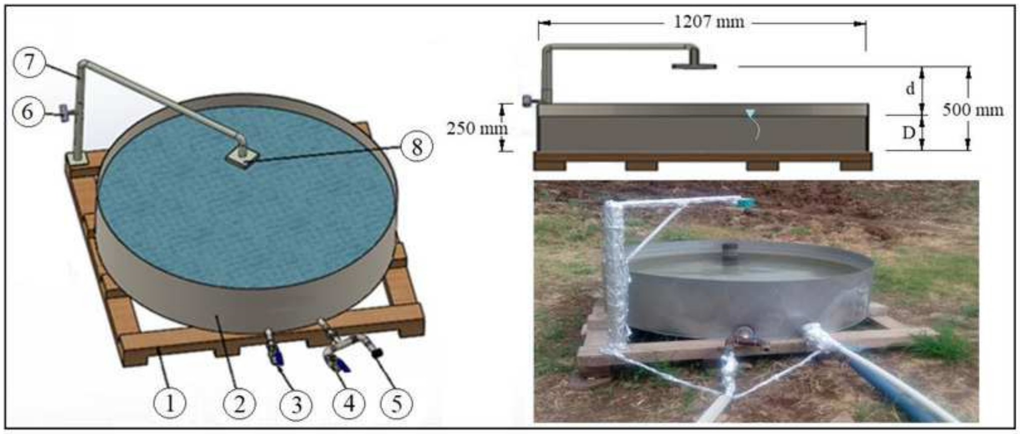

Figure 3 PLC controlled class-A pan evaporimeter. This evaporimeter (2) was sited on a 10 cm high wooden frame (1) placed on dry fallow soil surrounded by green crops. The pipes of the water inlet (3) and discharge (4) were placed on the bottom of the evaporimeter. Both of these pipes have a diameter of ½". A solenoid valve was connected to the water inlet pipe. The E_{pan} values can be measured separately by using a pressure sensor (5) placed on the discharge pipe or an ultrasonic sensor (8) sensitive to the water surface. The E_{pan} values measured by the ultrasonic sensor were used in this study. This sensor was placed at a height of 500 mm, coinciding with the centre of the evaporimeter, by means of a strut (7) with a height adjustment screw (6) on it.

Figure 4

Daily air temperature and relative humidity values for the July–October periods of 2020 and 2021.

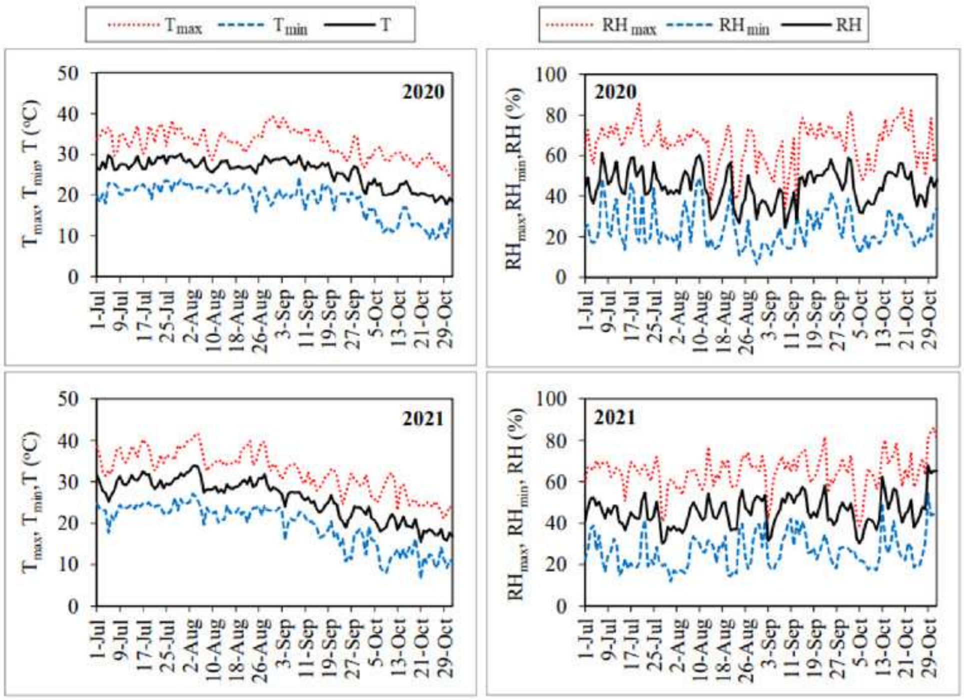

Figure 4 Daily air temperature and relative humidity values for the July–October periods of 2020 and 2021.

Figure 5

Daily average wind velocity and solar radiation values.

Each point on the graphs represents the daily average U_2 and R_s values for the July–October periods of 2020 and 2021.

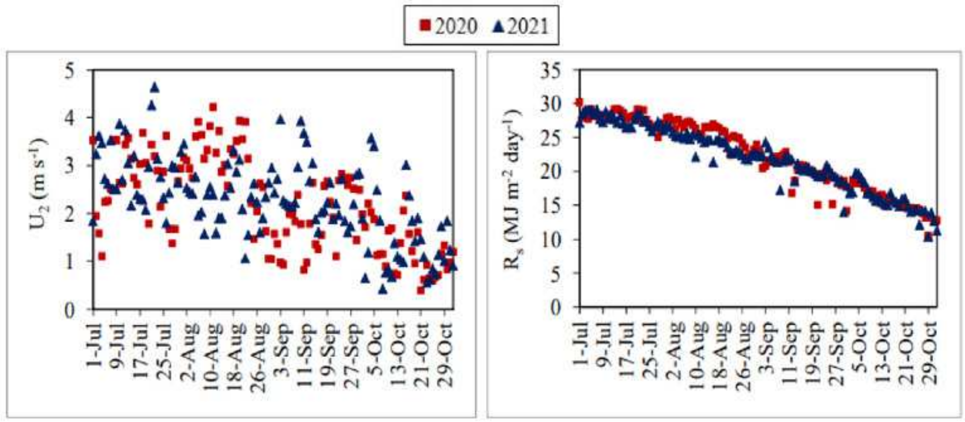

Figure 5 Daily average wind velocity and solar radiation values. Each point on the graphs represents the daily average U_2 and R_s values for the July–October periods of 2020 and 2021.

Figure 6

Daily average actual ET_o and daily total E_{pan} values.

Each point on the graphs represents the daily actual ET_o and E_{pan} values for the July–October periods of 2020 and 2021.

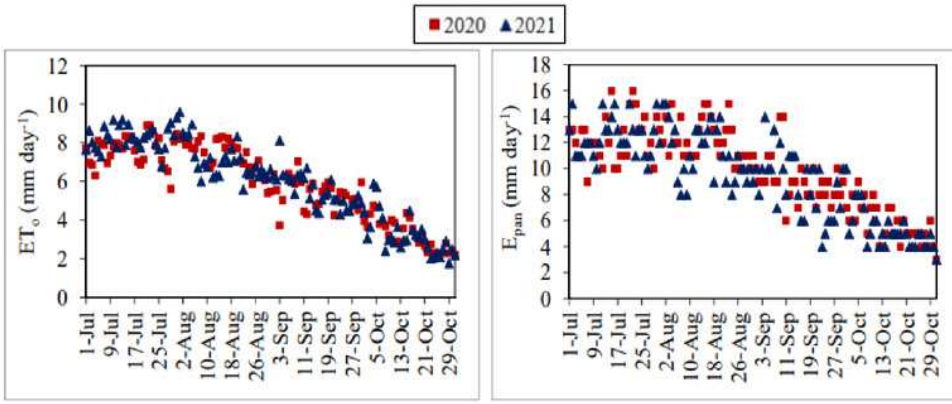

Figure 6 Daily average actual ET_o and daily total E_{pan} values. Each point on the graphs represents the daily actual ET_o and E_{pan} values for the July–October periods of 2020 and 2021.

Figure 7

Daily average actual and estimated K_p coefficients.

Each point on the graphs represents the daily K_p values for the July–October periods of 2020 and 2021.

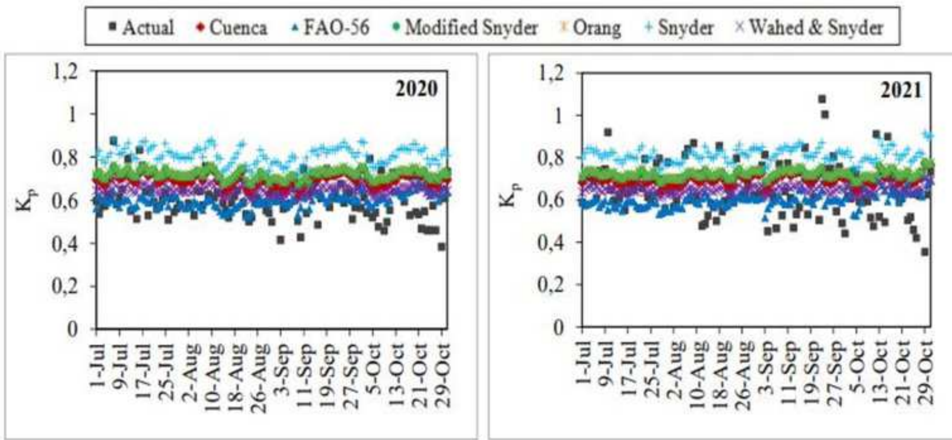

Figure 7 Daily average actual and estimated K_p coefficients. Each point on the graphs represents the daily K_p values for the July–October periods of 2020 and 2021.

Figure 8

Daily average actual and estimated ET_o values.

Each point on the graphs represents the actual and estimated ET_o values for the July–October periods of 2020 and 2021.

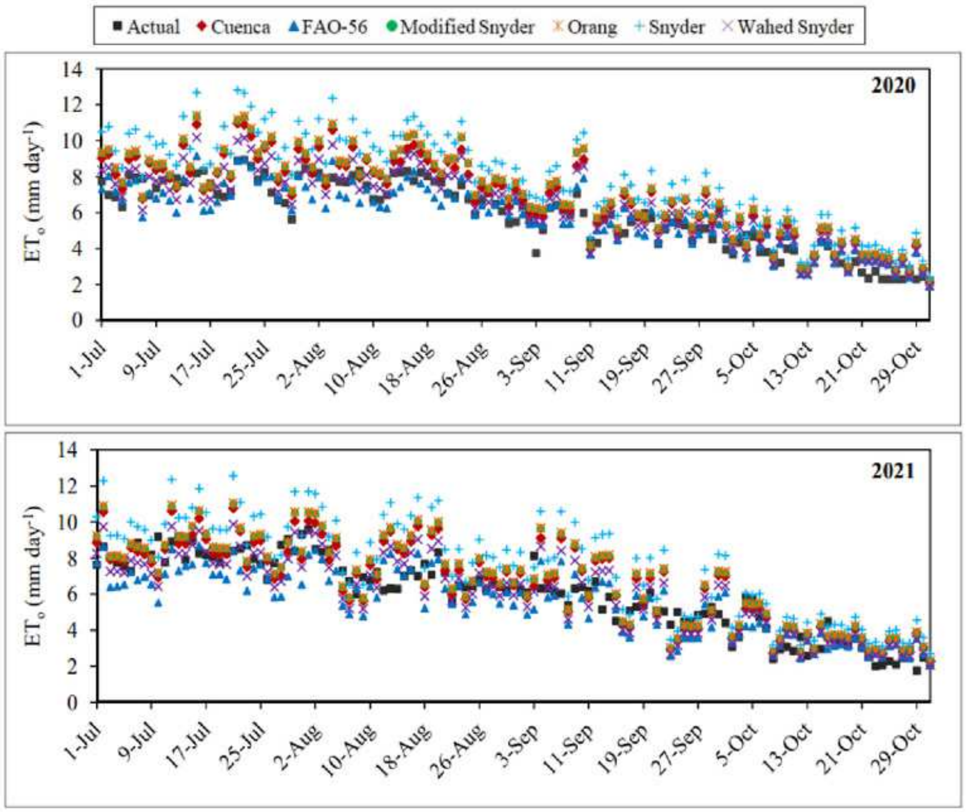

Figure 8 Daily average actual and estimated ET_o values. Each point on the graphs represents the actual and estimated ET_o values for the July–October periods of 2020 and 2021.

Figure 9

Statistical analysis of the relationship between actual and estimated daily average ET_o values (2020).

~~Each point on the graphs represents the actual and estimated daily average ET_o values for the July–October period of 2020.~~

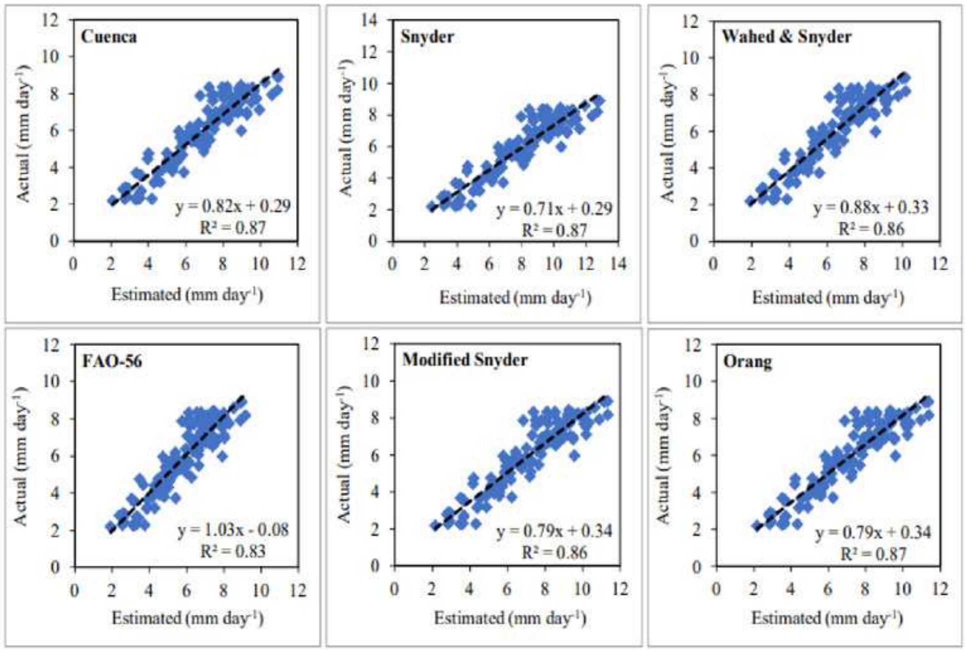

Figure 9 Statistical analysis of the relationship between actual and estimated daily average ET_o values (2020). Each point on the graphs represents the actual and estimated daily average ET_o values for the July–October period of 2020.

Figure 10

Statistical analysis of the relationship between actual and estimated daily average ET_o values (2021).

Each point on the graphs represents the actual and estimated daily average ET_o values for the July–October period of 2021.

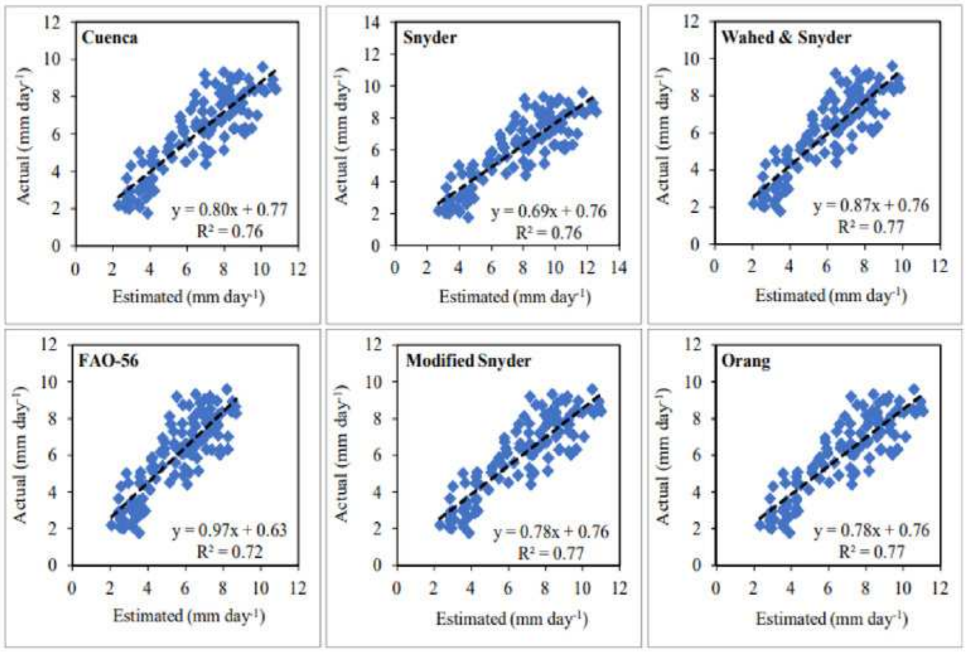

Figure 10 Statistical analysis of the relationship between actual and estimated daily average ET_o values (2021). Each point on the graphs represents the actual and estimated daily average ET_o values for the July–October period of 2021.

Figure 11

Monthly total actual and estimated ET_o values.

Each bar on the graphs represents the monthly total actual and estimated ET_o values for the July–October periods of 2020 and 2021.

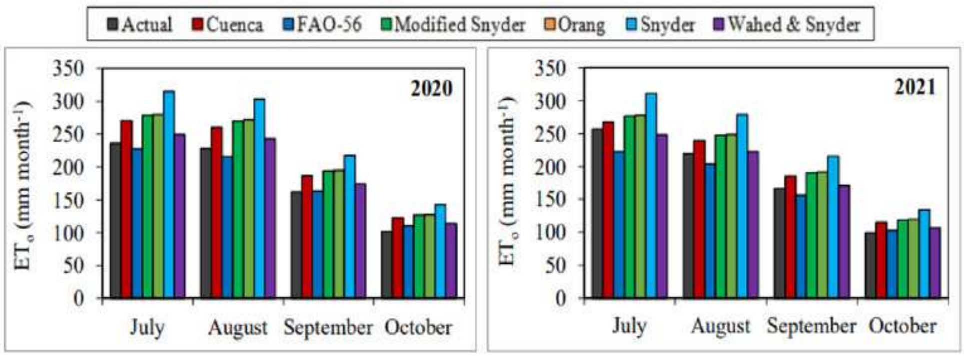

Figure 11. Monthly total actual and estimated ET_o values. Each bar on the graphs represents the monthly total actual and estimated ET_o values for the July–October periods of 2020 and 2021.

Table 1(on next page)

Class-A pan evaporimeter pan coefficient estimation models

K_p= class-A pan evaporimeter pan coefficient; U_2= wind velocity at 2 m above ground surface (m s^{-1}); RH= relative humidity (%); FET= class-A pan evaporimeter upwind buffer zone distance (m).

Table 1 Class-A pan evaporimeter pan coefficient estimation models

Model	Estimation equation
Cuenca	$K_p = 0.475 - 0.00024\ U_2 + 0.00516\ RH + 0.00118\ (FET) - 0.000016\ (RH)^2 - 0.00000101\ (FET)^2$ $0.000000008\ (RH)^2\ U_2 - 0.00000001\ (RH)^2\ (FET)$
Snyder	$K_p = 0.482 - 0.000376\ U_2 + 0.0424\ Ln(FET) + 0.0045\ RH$
Wahed & Snyder	$K_p = 0.62407 - 0.00028\ U_2 - 0.02660\ Ln(FET) + 0.00226\ RH$
FAO-56	$K_p = 0.61 + 0.000162\ U_2\ RH - 0.00000959\ U_2\ (FET) + 0.00341\ RH + 0.00327\ U_2\ Ln(FET) -$ $0.00289\ U_2\ Ln(86.4\ U_2) - 0.0106\ Ln(86.4\ U_2)\ Ln(FET) + 0.00063[Ln\ (FET)]^2\ Ln(86.4\ U_2)$
Modified Snyder	$K_p = 0.5321 - 0.0003\ U_2 + 0.0249\ Ln(FET) + 0.0025\ RH$
Orang	$K_p = 0.51206 - 0.000321\ U_2 + 0.03188\ Ln(FET) + 0.00289\ RH - 0.000107\ RH\ Ln(FET)$

Notes.

K_p= class-A pan evaporimeter pan coefficient; U_2= wind velocity at 2 m above ground surface (m s^{-1}); RH= relative humidity (%); FET= class-A pan evaporimeter upwind buffer zone distance (m).

Table 2(on next page)

Monthly averages of the actual and estimated daily K_p coefficients

Table 2 Monthly averages of the actual and estimated daily K_p coefficients

Model/Month (2020)	July	August	September	October	Average
Actual	0.62	0.60	0.61	0.58	0.60
Cuenca	0.71	0.69	0.69	0.69	0.70
Snyder	0.82	0.80	0.80	0.81	0.81
Wahed & Snyder	0.65	0.64	0.64	0.65	0.65
FAO-56	0.59	0.57	0.60	0.63	0.60
Modified Snyder	0.73	0.71	0.72	0.72	0.72
Orang	0.73	0.72	0.72	0.72	0.72
Model/Month (2021)	**July**	**August**	**September**	**October**	**Average**
Actual	0.67	0.65	0.67	0.61	0.65
Cuenca	0.69	0.70	0.71	0.70	0.70
Snyder	0.81	0.81	0.82	0.82	0.82
Wahed & Snyder	0.64	0.65	0.65	0.65	0.65
FAO-56	0.58	0.59	0.60	0.63	0.60
Modified Snyder	0.72	0.72	0.72	0.72	0.72
Orang	0.72	0.72	0.73	0.73	0.73

Table 3(on next page)

Monthly averages of the actual and estimated daily ET_o (mm day^{-1}) values

Table 3 Monthly averages of the actual and estimated daily ET_o (mm day^{-1}) values

Model/Month (2020)	July	August	September	October	Average
Actual	7.62	7.35	5.40	3.27	5.91
Cuenca	8.73	8.40	6.23	3.96	6.83
Snyder	10.17	9.78	7.26	4.61	7.96
Wahed & Snyder	8.06	7.83	5.81	3.68	6.35
FAO-56	7.33	6.98	5.43	3.56	5.83
Modified Snyder	8.97	8.72	6.46	4.09	7.07
Orang	9.02	8.77	6.50	4.11	7.10
Model/Month (2021)	**July**	**August**	**September**	**October**	**Average**
Actual	8.27	7.08	5.55	3.20	6.03
Cuenca	8.61	7.72	6.17	3.71	6.56
Snyder	10.02	8.98	7.19	4.32	7.63
Wahed & Snyder	8.00	7.16	5.70	3.44	6.08
FAO-56	7.17	6.58	5.22	3.30	5.57
Modified Snyder	8.91	7.98	6.34	3.83	6.77
Orang	8.95	8.02	6.38	3.85	6.80

Table 4(on next page)

MAE, MAPE and RMSE errors of the daily average estimated ET_o values

MAE, MAPE and RMSE errors express the deviation between the daily average actual ET_o values calculated using the FAO-56 PM equation and the daily average ET_o values estimated using the Cuenca, Snyder, Wahed & Snyder, FAO-56, Modified Snyder, and Orang models.

Table 4 MAE, MAPE and RMSE errors of the daily average estimated ET_o values

				Cuenca						
Month	**July**		**August**		**September**		**October**		**Average**	
Year	2020	2021	2020	2021	2020	2021	2020	2021	2020	2021
MAE (mm day^{-1})	1.31	0.97	1.10	1.08	0.88	1.18	0.80	0.72	1.02	0.99
MAPE (%)	17.52	11.65	15.32	15.66	17.10	21.32	25.55	25.20	18.87	18.46
RMSE (mm day^{-1})	1.49	1.17	1.25	1.35	1.13	1.47	0.93	0.91	1.22	1.24
				Snyder						
Month	**July**		**August**		**September**		**October**		**Average**	
Year	2020	2021	2020	2021	2020	2021	2020	2021	2020	2021
MAE (mm day^{-1})	2.55	1.86	2.43	1.96	1.86	1.82	1.35	1.17	2.05	1.71
MAPE (%)	33.99	22.91	33.58	28.35	35.07	32.57	42.95	41.82	36.40	31.41
RMSE (mm day^{-1})	2.79	2.16	2.56	2.34	2.06	2.27	1.53	1.39	2.28	2.08
Model					**Wahed & Snyder**					
Month	**July**		**August**		**September**		**October**		**Average**	
Year	2020	2021	2020	2021	2020	2021	2020	2021	2020	2021
MAE (mm day^{-1})	0.90	0.86	0.71	0.91	0.62	1.03	0.64	0.56	0.71	0.84
MAPE (%)	11.86	10.11	9.82	13.01	11.89	18.86	20.52	19.14	13.52	15.28
RMSE (mm day^{-1})	1.05	1.06	0.84	1.10	0.85	1.22	0.72	0.75	0.87	1.06
				FAO-56						
Month	**July**		**August**		**September**		**October**		**Average**	
Year	2020	2021	2020	2021	2020	2021	2020	2021	2020	2021
MAE (mm day^{-1})	0.68	1.15	0.66	0.95	0.56	1.02	0.56	0.60	0.62	0.93
MAPE (%)	8.96	13.47	8.79	13.33	10.73	18.60	18.78	19.68	11.81	16.28
RMSE (mm day^{-1})	0.93	1.50	0.81	1.20	0.73	1.19	0.66	0.82	0.79	1.20
				Modified Snyder						
Month	**July**		**August**		**September**		**October**		**Average**	
Year	2020	2021	2020	2021	2020	2021	2020	2021	2020	2021
MAE (mm day^{-1})	1.52	1.05	1.39	1.22	1.09	1.24	0.88	0.78	1.22	1.07
MAPE (%)	20.22	12.77	19.40	17.60	20.87	22.31	28.23	27.60	22.18	20.07
RMSE (mm day^{-1})	1.71	1.28	1.56	1.51	1.35	1.575	1.06	0.98	1.44	1.36
				Orang						
Month	**July**		**August**		**September**		**October**		**Average**	
Year	2020	2021	2020	2021	2020	2021	2020	2021	2020	2021
MAE (mm day^{-1})	1.55	1.08	1.43	1.24	1.12	1.26	0.90	0.80	1.25	1.09
MAPE (%)	20.73	13.09	19.95	17.98	21.44	22.60	28.74	28.15	22.72	20.45
RMSE (mm day^{-1})	1.75	1.31	1.60	1.54	1.38	1.60	1.07	0.99	1.47	1.38

Notes.

MAE, MAPE and RMSE errors express the deviation between the daily average actual ET_o values calculated using the FAO-56 PM equation and the daily average ET_o values estimated using the Cuenca, Snyder, Wahed & Snyder, FAO-56, Modified Snyder, and Orang models.

Table 5 (on next page)

MAE and MAPE errors of the seasonal total ET_o values estimated using the models

MAE and MAPE errors express the deviation between the actual seasonal total ET_o value calculated using the FAO-56 PM equation and the seasonal total ET_o values estimated using the Cuenca, Snyder, Wahed & Snyder, FAO-56, Modified Snyder, and Orang models.

Table 5 MAE and MAPE errors of the seasonal total ET_o values estimated using the models

Model/Year	2020		2021	
	MAE (mm)	MAPE (%)	MAE (mm)	MAPE (%)
Cuenca	113.11	15.55	64.84	8.75
Snyder	251.65	34.60	197.27	26.61
Wahed & Snyder	53.36	7.34	6.16	0.83
FAO-56	10.58	1.45	56.13	7.57
Modified Snyder	141.76	19.45	90.80	12.25
Orang	146.43	20.13	95.31	12.85

Notes.

MAE and MAPE errors express the deviation between the actual seasonal total ET_o value calculated using the FAO-56 PM equation and the seasonal total ET_o values estimated using the Cuenca, Snyder, Wahed & Snyder, FAO-56, Modified Snyder, and Orang models.